Resource

Cell Chemical Biology

Acid-Tolerant Monomeric GFP from *Olindias formosa*

Graphical Abstract

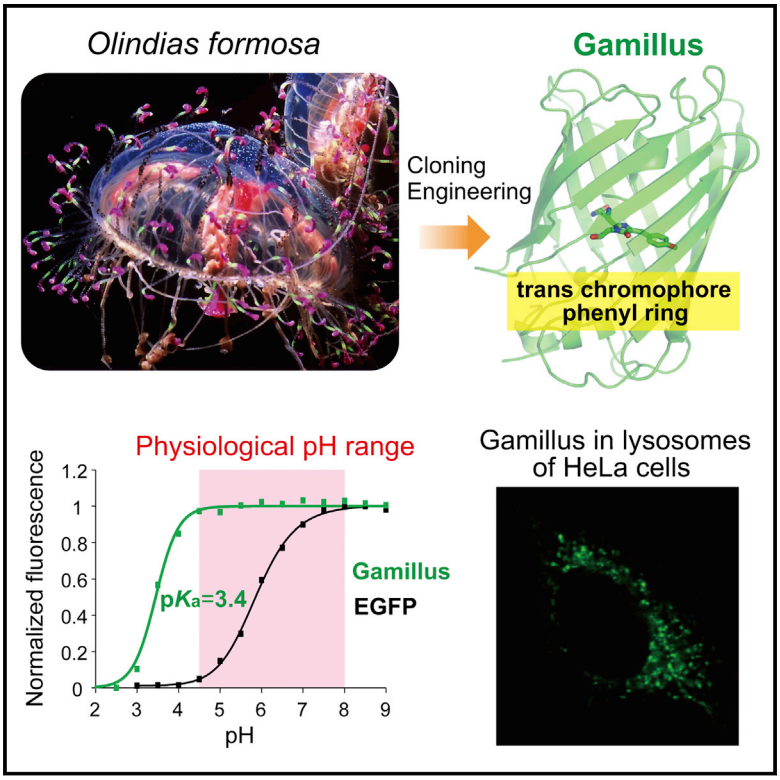

Highlights

- The acid-tolerant monomeric GFP "Gamillus" has pK_a of 3.4
- Gamillus shows excellent brightness, chromophore maturation speed, and photostability
- Gamillus adapts *trans* isomeric conformation of the chromophore phenyl ring
- Gamillus is a good molecular tag for studying biological event in acidic compartment

Authors

Hajime Shinoda, Yuanqing Ma, Ryosuke Nakashima, Keisuke Sakurai, Tomoki Matsuda, Takeharu Nagai

Correspondence

ng1@sanken.osaka-u.ac.jp

In Brief

Shinoda et al. describe the cloning, engineering, and characterization of a monomeric GFP "Gamillus" from *Olindias formosa*. Gamillus has superior acid tolerance (pK_a = 3.4) to reported other monomeric GFPs, and a unique *trans* chromophore configuration contributed to the acid tolerance. They demonstrate the usefulness for imaging in an acidic cellular environment, e.g., lysosomes.

Shinoda et al., 2018, Cell Chemical Biology *25*, 330–338
March 15, 2018
https://doi.org/10.1016/j.chembiol.2017.12.005

CellPress

CellPress

Cell Chemical Biology
Resource

Acid-Tolerant Monomeric GFP from *Olindias formosa*

Hajime Shinoda,[1] Yuanqing Ma,[1,3] Ryosuke Nakashima,[2] Keisuke Sakurai,[2] Tomoki Matsuda,[1,2] and Takeharu Nagai[1,2,4,*]
[1]Department of Biotechnology, Graduate School of Engineering, Osaka University, 2-1 Yamadaoka, Suita 565-0871, Japan
[2]The Institute of Scientific and Industrial Research, Osaka University, 8-1 Mihogaoka, Ibaraki 567-0047, Japan
[3]Present address: EMBL Australia Node in Single Molecule Science, School of Medical Sciences, University of New South Wales, Sydney, NSW 2052, Australia
[4]Lead Contact
*Correspondence: ng1@sanken.osaka-u.ac.jp
https://doi.org/10.1016/j.chembiol.2017.12.005

SUMMARY

The fluorescent protein (FP) color palette has greatly contributed to the visualization of molecular and cellular processes. However, most FPs lose fluorescence at a pH lower than their neutral pK_a (~6), and this has hampered their application in acidic organelles (pH ~4.5–6.0). Currently, several cyan- and red-colored acid-tolerant FPs are available; however, there are few reports of acid-tolerant green FPs (GFPs) that are practically applicable to bioimaging. Here, we developed the acid-tolerant monomeric GFP "Gamillus" from the jellyfish *Olindias formosa*, with excellent brightness, maturation speed, and photostability. Results from X-ray crystallography and point mutagenesis suggest that across a broad pH range the acid tolerance is attributed to stabilization of deprotonation in the chromophore phenyl ring by forming a unique *trans* configuration. We demonstrate that Gamillus can serve as a molecular tag suitable for imaging in acidic organelles through autophagy-mediated molecular tracking to lysosomes.

INTRODUCTION

Acidic organelles, such as endosomes, secretory granules, lysosomes, and plant vacuoles, are transit points or terminals for sorting, modification, transport, and degradation of biomolecules (Huotari and Helenius, 2011). Recently, important roles as signaling centers for essential physiological functions have been revealed, including autophagy, apoptosis, and plasma membrane repair (Settembre et al., 2013). Multiple proteins (e.g., cathepsin B and cathepsin D) and ions (e.g., H^+, Ca^{2+}, and Cl^-) stored inside acidic organelles have been expected to be key factors in the regulation of these functions (Boya and Kroemer, 2008; Settembre et al., 2013). Fluorescent proteins (FPs) could potentially be one of the most powerful tools to investigate molecular dynamics inside acidic organelles (Tsien, 1998). However, in most cases FPs have usage limitations for imaging in acidic organelles as they lose fluorescence in pH environments below their neutral fluorescence pK_a (~6), caused by chromophore protonation (Cranfill et al., 2016). Only a small number of reported acid-tolerant FPs, such as Sirius (ultramarine FP, pK_a < 3.0) (Tomosugi et al., 2009), mTurquoise2 (cyan FP, pK_a = 3.1) (Goedhart et al., 2012), and TagRFP (red FP, pK_a = 3.8) (Merzlyak et al., 2007), allow labeling and monitoring of specific proteins in acidic organelles. To understand the detailed relationships between multiple proteins, multicolor imaging with FPs of different colors is desirable. However, there is a lack of appropriate acid-tolerant green FPs (GFPs). Although there are reports of several acid-tolerant GFPs, most have serious drawbacks. For example, CpYGFP (pK_a = 4.4) (Masuda et al., 2006) and bfloGFPa1 (pK_a = 4.0) (Bomati et al., 2014) form homodimers or homotetramers under physiological conditions, possibly causing mislocalization or dysfunction of the fused proteins (Ai et al., 2014). Meanwhile, monomeric enhanced cyan-green FP (ECGFP) (pK_a < 4.0) is 10-fold less bright than the enhanced GFP (EGFP) used regularly in non-acidic environments (Sawano and Miyawaki, 2000). To overcome the challenges in the application of GFPs for multicolor imaging in acidic organelles, here we report an acid-tolerant monomeric GFP that is practically applicable to live-cell imaging in acidic organelles.

RESULTS AND DISCUSSION

Molecular Cloning of Acid-Tolerant GFP from Flower Hat Jellyfish

The tentacle sections from the flower hat jellyfish (*Olindias formosa*) that emit strong green fluorescence were investigated for unidentified GFP genes (Figure 1). In brief, an *Escherichia coli* cDNA expression library was constructed from jellyfish mRNA. Several green fluorescent colonies were isolated from a pool of ~20,000 colonies, leading to the identification of a novel GFP, designated dfGFP, sharing little similarity to the known FPs. For instance, it displayed 65%, 44%, and 33% homology to Ember (Hunt et al., 2012), anm2CP (origin of KillerRed [Shagin et al., 2004]) and avGFP (origin of EGFP [Shimomura et al., 1962]), respectively (Figure S1). The use of pH titration revealed that dfGFP has surprisingly high acid tolerance (pK_a = 3.8) (Figures S2A and S2B), and was therefore used as a template to develop an acid-tolerant GFP for bioimaging. An inherent problem with dfGFP is a tendency for dimer formation under physiological concentrations, as shown by size-exclusion chromatography (Figure S2C). Beyond dimerization problems, purified dfGFP had a tendency to aggregate in solution (detected by visual observation), where aggregation can cause fused protein defects that lead to cell toxicity (Yanushevich et al.,

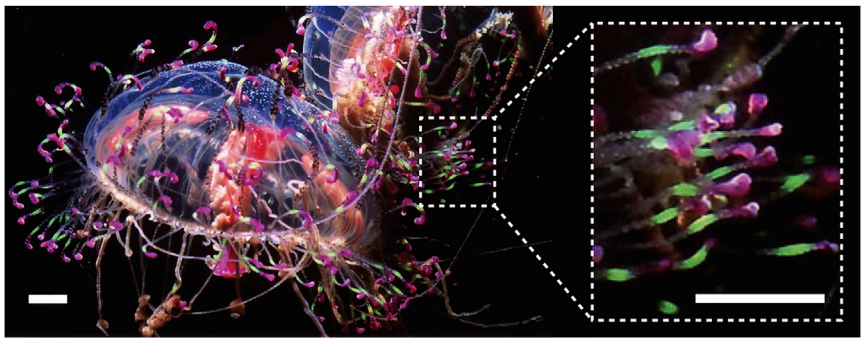

Figure 1. Flower Hat Jellyfish (*Olindias formosa*)
Scale bars, 1 cm. See also Figure S1.

2002). These problems were resolved using protein engineering, with a combination of rational design and directed evolution (Ai et al., 2014; Hoi et al., 2013; Shaner et al., 2013).

Directed Evolution of dfGFP for Improved Monomeric Property, Solubility, and Brightness

First, we monomerized dfGFP by following a commonly used strategy (Ai et al., 2014; Hoi et al., 2013; Shaner et al., 2013). A homology model of the monomeric dfGFP structure was calculated using the SWISS-MODEL server (Bordoli et al., 2009), and two molecules were superimposed onto a published KillerRed dimeric structure (PDB: 3wck) (Takemoto et al., 2013) (Figure S3A). Hydrophobic dimer interface residues were substituted with neutral amino acids with short side chains or a positively charged arginine (F149T, L158T, H160T, Y174R, and Y192A) in order to disrupt dimer formation, which was confirmed by size-exclusion chromatography. The brightness of the first monomeric version of dfGFP, Gamillus0.1, was relatively low ($\varepsilon = 20\ mM^{-1}\ cm^{-1}$; $\Phi = 0.84$; $pK_a < 4$). To restore the brightness lost by monomerization, we applied a round of random mutagenesis to screen for variants with brighter fluorescence as observed in bacterial colonies. In all of the following screening processes the fluorescence pK_a was measured, and the variants with a pK_a less than 4.0 were selected for further mutagenesis. The resulting Gamillus0.2 (with an additional P162L mutation along with the original Gamillus0.1 mutations) had an almost 2-fold increase in brightness and good acid tolerance ($\varepsilon = 55\ mM^{-1}\ cm^{-1}$; $\Phi = 0.94$), although it forms a weak dimer. To further disturb dimer interaction, we introduced another substitution at the 174th residue, situated at the dimer interface of Gamillus0.2. An additional R174T substitution resulted in Gamillus0.3 that harbored an enhanced monomeric property ($\varepsilon = 51\ mM^{-1}\ cm^{-1}$; $\Phi = 0.88$). To further improve brightness, we conducted three rounds of random mutagenesis using the bacterial screening system and combined the obtained mutations together. The resultant variant, Gamillus0.4 (with additional mutations N37S, K112E, E147K, K185R, and P223L), displayed higher fluorescence signals *in vitro* ($\varepsilon = 75\ mM^{-1}\ cm^{-1}$; $\Phi = 0.89$) and faster chromophore formation in bacteria at 37°C. During this process, a slightly improved solubility was observed with the K112E surface mutation. This suggested that the aggregation of dfGFP presumably caused by nonspecific electrostatic interaction could be alleviated by amino acid substitution of surface residues (Evdokimov et al., 2006; Lawrence et al., 2007). Based on the electrostatic potential map of Gamillus0.4 model, residues around the positively charged surface were substituted to negatively charged ones (Q145E and K166E), whereby the Gamillus0.5 variant resulted in significantly less aggregation in solution. The Gamillus0.5 variant also contains the E140K substitution for improved brightness, which was identified during rounds of random mutagenesis and the bacterial screening. When Gamillus0.5 was expressed in the cytosol of HeLa cells, the fluorescence was much dimmer when compared with cells expressing EGFP. To investigate, we aligned the Gamillus0.5 homology-modeled structure and compared with the reported KillerRed and EGFP (PDB: 2y0g) crystal structures. For Gamillus0.5, a relatively shorter loop structure between its seventh and eighth β sheets was identified when compared with the other structures. Presumably, this causes a slight distortion of the β-barrel structure and might influence the configuration of the side-chain residues around the chromophore. This may directly reduce the efficiency of chromophore maturation, resulting in dimmer fluorescence emissions in HeLa cells. Following this hypothesis, the short loop of Gamillus0.5 was substituted with the longer one found in KillerRed (i.e., changing AEG at positions 150–152 to PHGP), and the neighboring 180th amino acid was replaced with the equivalent in KillerRed (K180T). These substitutions successfully improved the maturation speed and resulted in the final variant with an approximately 3-fold increase in brightness in HeLa cells ($\varepsilon = 83\ mM^{-1}\ cm^{-1}$; $\Phi = 0.90$; $pK_a = 3.4$ with *in vitro* characteristics). The final variant was designated as Gamillus, an abbreviation of "**G**FP with **a**cid tolerance and **m**onomeric properties to **illu**minate **s**oured environments." In total, Gamillus contains 18 point mutations, where side chains are directed to the outside of the β barrel, and includes EGFP-type N and C termini (Figures 2 and S3B).

Characterization of Gamillus

The photophysical properties of Gamillus were compared with those of EGFP, one of the most commonly used GFPs (Table 1). Spectroscopic measurements revealed that Gamillus has sharp excitation and emission peaks at 504 nm and 519 nm respectively, which are shifted to slightly longer wavelengths than for EGFP (488 nm and 507 nm). The extinction coefficient ($83\ mM^{-1}\ cm^{-1}$; Figure S4A) and fluorescence quantum yield (0.90; Table S1) of Gamillus makes it 1.78 times brighter than EGFP. To the best of our knowledge, this is the highest quantum yield of all reported monomeric GFPs. The oxygen-dependent chromophore maturation rate of Gamillus at 37°C was 1.6 times larger than that of EGFP (Figure S4B). The maturation efficiency of Gamillus expressed and purified from bacteria (58%) was somewhat lower than that of EGFP (66%). Cytotoxicity of Gamillus was assessed by observation of FP expressing HeLa cell number over 2 days. This assay indicates that Gamillus has a slightly higher toxicity than EGFP (Figure S4C). Monomeric state under physiological concentrations (<50 μM) was verified by

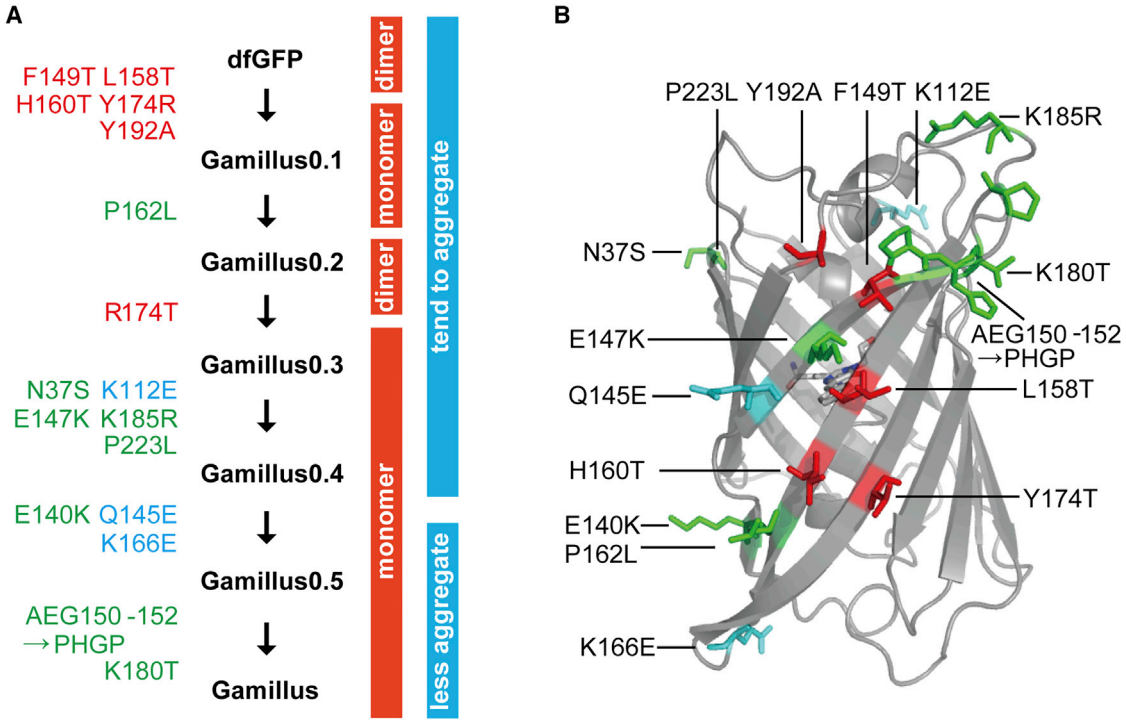

Figure 2. Engineering of Gamillus from dfGFP

(A) Lineage of Gamillus.

(B) Positions of substituted amino acids during the directed evolution process, depicted on the X-ray crystal structure of Gamillus. Generally, the mutations for monomerization are represented in red, those for improvement of brightness are in green, and those for improvement of solubility are in blue.

See also Figures S2 and S3.

size-exclusion chromatography (Figure S4D). In addition, monomerization under physiological conditions was characterized with the "organized smooth ER" (OSER) assay (Costantini et al., 2012). In this assay, FPs fused on the cytoplasmic end of ER membrane protein (CytERM) are expressed in cells, where FPs exhibiting oligomeric tendency interact with FPs on an opposite ER membrane, leading to restructuring of the ER from a tubular network into OSER whorl structures. This analysis revealed that whorl-free HeLa cells transfected with CytERM-Gamillus was 89%, compared with the value obtained with weak dimeric EGFP (84%) or monomeric mNeonGreen (90%) (Figure S4K).

Next, the photochromic behavior of Gamillus was investigated. *In vitro* experiments revealed that the major absorption peak of Gamillus is shifted from 502 nm to 388 nm by irradiation with 500–525 nm light, and returned to 502 nm by irradiation with 375–398 nm light (data not shown). The absorption peaks at 502 nm and 388 nm are probably attributed to ionic and neutral state of the chromophore, respectively. A similar spectral change is observed in general reversibly photoswitching FPs (rsFPs) such as Dronpa (Ando et al., 2004) and rsEGFP (Bizzarri et al., 2010). Since their change is related to ionic and neutral states of the chromophore that is accompanied with *cis-trans* isomerization, the spectral change of Gamillus is also likely to

Table 1. Photophysical Properties of Gamillus and EGFP

Protein	$\lambda_{ex}/\lambda_{em}$[a] (nm)	ε[b] (mM^{-1} cm^{-1})	Φ[c]	Brightness[d] (*In Vitro*)	Brightness[e] (HeLa Cell)	pK_a[f]	Photostability[g] (min)	Maturation[h] (min)	Mature Fraction[i] (%)
Gamillus	504/519	83	0.90	178	52	3.4	1.22	8.0	58
EGFP	488/507	56	0.75	100	100	5.9	0.59	14.9	66

See also Figures S4 and S5; Table S1.

[a]Excitation and emission peak.

[b]Molar extinction coefficient determined by alkali-denaturation method.

[c]Absolute fluorescence quantum yield determined by integrating sphere.

[d]Product of ε and Φ, indicated as a percentage of brightness of EGFP.

[e]Average brightness in HeLa cells, indicated as a percentage of EGFP.

[f]pH at which fluorescence intensity becomes its half-maximal value.

[g]Photobleaching half-time in live HeLa cells under 440–480 nm mercury arc illumination.

[h]Half-time required for the chromophore formation in oxygen-dependent manner.

[i]Percentage of matured chromophore of total purified protein collected from bacterial lysates.

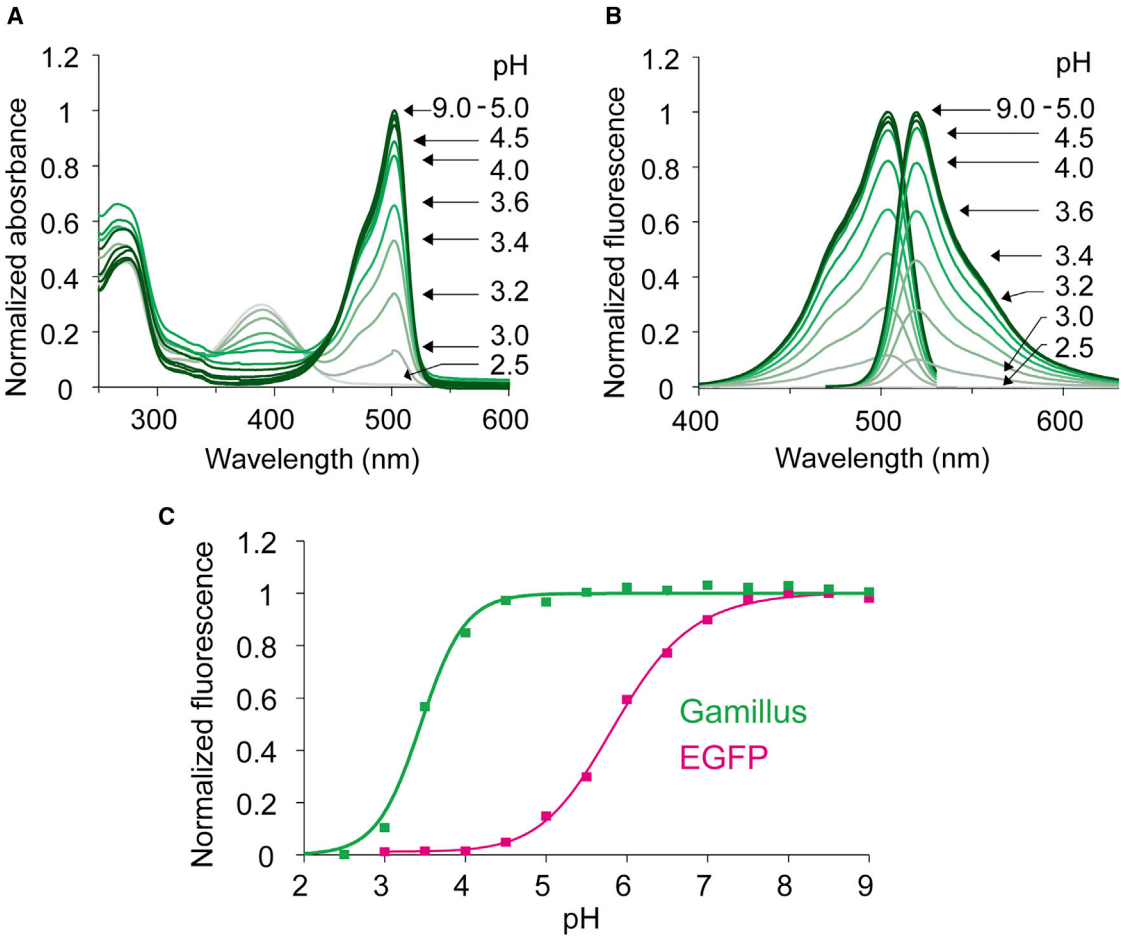

Figure 3. *In Vitro* Characterization of pH-Dependent Fluorescence Properties of Gamillus

(A and B) Absorption (A) and excitation/emission spectra (B) of purified Gamillus in the range from pH 2.5 to 9.0. Data was normalized using the maximum value in pH 9.0 solution.

(C) The pH-titration curve for fluorescence emission of purified Gamillus and EGFP (n = 3).

be caused by a similar mechanism. To explore this hypothesis, detailed analysis of the off state of Gamillus through further experiments such as X-ray crystallography will be necessary. Gamillus expressed in HeLa cells also exhibited a photochromic decrease in fluorescence to ~60% or ~10% of its initial intensity by exciting with 457–487 nm (GFP excitation range, 470 mW/cm^2 for 40 s) or 488–512 nm (YFP excitation range, 360 mW/cm^2 for 40 s) mercury arc light, respectively. The decreased intensity was recovered by subsequent irradiation with 352–388 nm light (770 mW/cm^2 for 10 s). In contrast, such time-dependent fluorescence intensity changes were negligible using 440–480 nm excitation light (Figures S4E and S4F) as it presumably renders photochromic equilibrium of Gamillus dominant in the ionic state. Under these conditions, the overlap between the spectra for excitation and the absorption for chromophore switching-on (from the neutral to the ionic state) is narrow. Thus, equilibrium between on and off states is unlikely to be achieved. One of the possible reasons for the negligible photochromism is a much higher on-switching rate, compared with the switching-off rate. In our estimation, the switching-on rate is ~200-fold higher than switching-off with 405 nm and 488 nm laser illumination, at the same power density. Another possibility is that the spectral edge of the bandpass filter (465AF30) used for the 440–480 nm excitation may allow some of the 436 nm emission of the mercury arc lamp to leak into the excitation light. To simplify imaging we therefore selected 440–480 nm illumination to limit the photochromic phenomena. Under this excitation wavelength range, the *in vitro* brightness of Gamillus (calculated as the product of averaged extinction coefficients over 440–480 nm [$\varepsilon_{440\text{-}480}$] and quantum yield) is 98% of that of EGFP ($\varepsilon_{440\text{-}480}$ for Gamillus and EGFP were 28.8 and 35.4 mM^{-1} cm^{-1}, respectively). In contrast, the average brightness of Gamillus expressed in HeLa cells was 52% of that of EGFP (Figure S4G), possibly due to reduced maturation efficiency or a lower expression. However, using the same power density of 440–480 nm illumination, Gamillus displayed 2-fold higher photostability than EGFP in HeLa cells (Figure S4H).

The pH-dependent fluorescence properties of Gamillus were investigated in increments between pH 2.5 and 9.0. Notably, the intensities for absorption, excitation, and emission spectra were essentially constant between pH 4.5 and 9.0 (Figure 3), within the intracellular pH range in most cell types (Casey

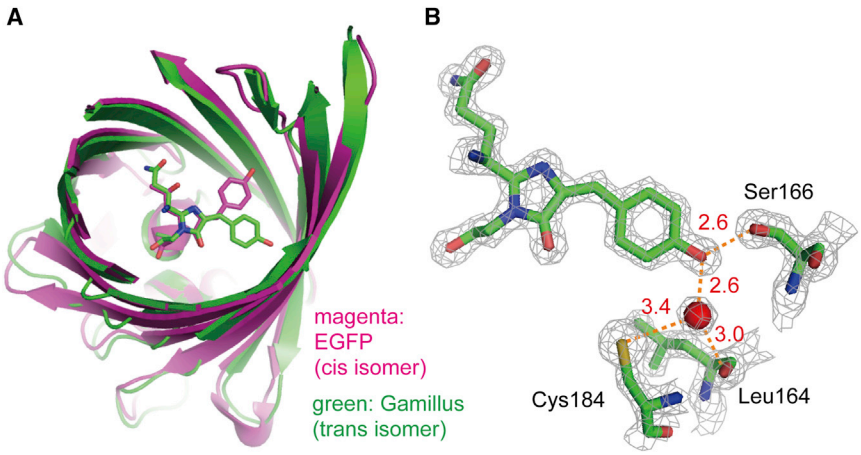

Figure 4. Molecular Structure of Gamillus Determined by X-Ray Crystallography

(A) Superimposed structures of Gamillus (green; PDB: 5y00) and EGFP (magenta; PDB: 2y0g).

(B) Close-up view of the chromophore site of Gamillus. The electron density map ($2F_o$-F_c) contoured at 2.0σ is depicted as gray mesh; amino acids are represented as a stick model (green, carbon; red, oxygen; blue, nitrogen; yellow, sulfide); main-chain traces are drawn as cartoon β sheets; water molecules are represented by red spheres; and hydrogen bonds are represented by orange dots (lengths in angstroms). See also Figure S6 and Table S2.

et al., 2010). With a pH below 4.5, the intensities of the excitation and emission spectra decreased. The intensities for the absorbance peak at 504 nm and the non-excitable peak at 390 nm were decreased and increased, respectively, likely due to protonation of the chromophore (Tsien, 1998). Compared with other GFPs, Gamillus exhibited superior acid tolerance (pK_a = 3.4; Figure S5). The long-term stability of GFPs in acidic conditions was also characterized. After 24 hr incubation at pH 4.5, EGFP completely lost fluorescence, while fluorescence loss for Gamillus was smaller (Figure S4I). Additionally, compared with EGFP, Gamillus had superior long-term stability in a solution containing strong denaturant (4.0–6.2 M guanidine hydrochloride) (Figure S4J).

Molecular Structure and Suggested Mechanism for Acid Tolerance of Gamillus

To investigate the structural basis of acid-tolerance mechanisms, we determined the crystal structure of Gamillus at pH 5.5. The electron density map shows that Gamillus has a chromophore hydroxyphenyl ring in the *trans* configuration, unlike that found the currently published structures of GFPs that display the *cis* configuration in the fluorescence state (Figure 4A). The chromophore phenolate oxygen of Gamillus forms hydrogen bonds with a water molecule and the side chain of Ser166, stabilizing the phenolic ring (Figure 4B). Because this water molecule is separate from the bulk water (Figure S6A), the hydrogen bond with the chromophore phenolate oxygen would be stable across broad pH ranges. In addition, the chromophore phenolic ring is stacked with Gln182 that is stabilized by hydrogen bonds with the neighboring Ser67 side chain (Figure S6B). Gln182 could potentially stabilize the *trans* conformation by acting as a barrier for chromophore rotation. In fact, point mutations at the Gln182 residue (Q182N and Q182L) resulted in increased pH sensitivity, with a pK_a of 4.9 and 5.8, respectively (Figure S6C). The crystal structure of Gamillus at pH 3.0 revealed the predominant existence of the *cis* chromophore (Figure S6D). These results suggest that loss of fluorescence for Gamillus is accompanied by *trans-cis* isomerization of the chromophore, where stabilization of the *trans* conformation by the Gln182 residue is important to the acid-tolerance property.

Performance of Gamillus as a Molecular Tag

To confirm the applicability of Gamillus as a fluorescent tag for live-cell imaging, we constructed fusions of Gamillus with signal peptides and targeting proteins. Gamillus fusions showed expected localization in various organelles and cellular structures, including β-tubulin and histone 2B (H2B), which require a high degree of monomerization (Ai et al., 2014) (Figure 5). Gamillus fused to the luminal loop domain of lysosome-associated membrane protein 3 (LAMP3) (Rost et al., 2015) also showed the expected localization at the lysosome (Figure 5O), the most acidic organelle (pH ~4.5–5.0) containing multiple denaturation enzymes (Mindell, 2012). Compared with EGFP fused to LAMP3, Gamillus displayed 4.1-fold higher fluorescence signals on average (Figures S7A and S7B). Followed by alkalization of the lysosomal lumen with ammonium chloride, the fluorescence intensity of Gamillus remained constant (i.e., less than 5% increase), while that of EGFP increased by ~300% due to its neutral fluorescence pK_a (Figures S7C and S7E). Overall, Gamillus has clear advantages for imaging in acidic cellular environments. Some fusions of Gamillus with target proteins such as H2B, LifeAct, PTS1 sequence (peroxisome), CoxVIII signal sequence (mitochondria), and β1,4-galactosyltransferase (Golgi complex) exhibited normal localization even 3 days after transfection, while other fusions with β-tubulin, β-actin, fibrillarin, lyn, zyxin, or paxillin exhibited a tendency of accumulation in lysosomes presumably due to protein delivery by macroautophagy or endo-/exosomal activity (Figure S7F). This indicates that preliminary checking for lysosomal accumulation is indispensable when Gamillus is used as a fusion tag for target proteins.

Gamillus for Imaging Biological Events Occurring in Acidic Organelles

The utility of Gamillus for molecular tracking in autophagic events was also demonstrated. It has been reported that FPs without any fusion tags that are expressed in cytosol are delivered into lysosomes by macroautophagy (Katayama et al., 2008). Only FPs tolerant to acidic and proteolytic degradation, such as mRFP1(Campbell et al., 2002), can emit fluorescence in lysosomes (Katayama et al., 2008). For Gamillus, 2–3 days after gene transfection in HeLa cells a dot-like fluorescence pattern gradually appeared that colocalized with the lysosome

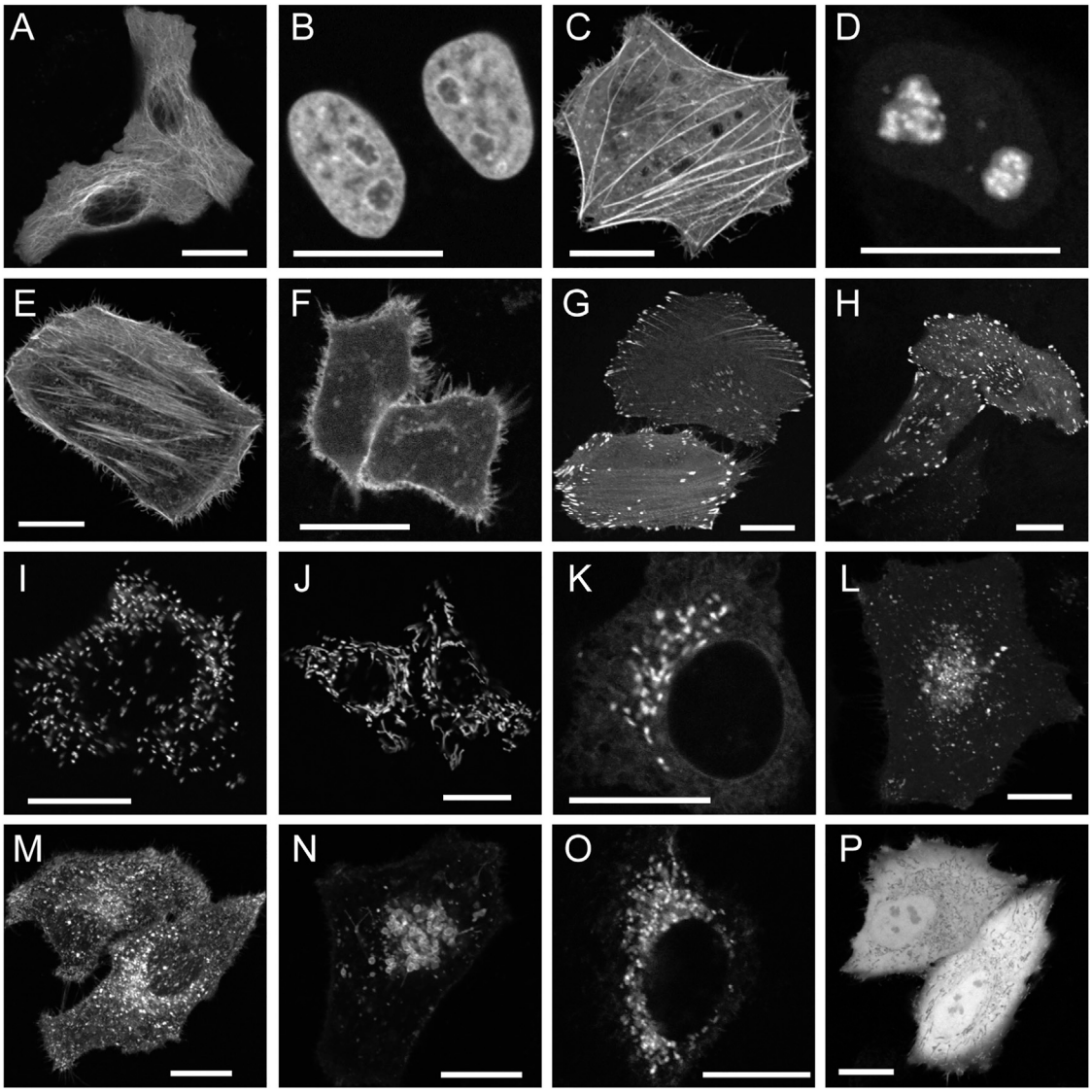

Figure 5. Fluorescence Localization

Fluorescence localization images of Gamillus fused to (A) β-tubulin (microtubule), (B) H2B (nucleus), (C) β-actin (cytoskeleton), (D) fibrillarin (nucleoli), (E) LifeAct (cytoskeleton), (F) lyn (inner plasma membrane), (G) zyxin (focal adhesions), (H) paxillin (focal adhesions), (I) PTS1 sequence (peroxisome), (J) CoxVIII signal sequence (mitochondria), (K) β1,4-galactosyltransferase (Golgi complex), (L) LC3 (autophagosome), (M) VAMP2 (secretory granule), (N) LAMP1 (external of lysosome), (O) LAMP3 (internal of lysosome), and (P) non-fused Gamillus. Scale bars, 20 μm.

marker (LysoTracker red) (Figure 6 and Movie S1). In contrast, EGFP and mNeonGreen (pK_a = 5.1), being less stable in acidic and proteolytic environments, had lower fluorescence intensity in the lysosome than in the cytosol. Accordingly, Gamillus has great potential to facilitate investigating biological events occurring in acidic organelles, such as molecular transport by endosomes and exosomes or intracellular signaling initiated by protein release from acidic organelles.

SIGNIFICANCE

The Gamillus protein is an acid-tolerant monomeric GFP cloned from flower hat jellyfish and engineered for bioimaging applications. Gamillus exhibits superior acid tolerance (pK_a = 3.4) to the reported GFPs; the fluorescence spectrum is essentially constant between pH 4.5 and 9.0, within the intracellular pH range in most cell types. The results of X-ray crystallography and mutagenesis studies suggest that the acid tolerance is attributable to the stabilization of the unique *trans* configuration of the chromophore phenyl ring. In comparison with conventional EGFP, Gamillus exhibits 1.8 times higher *in vitro* brightness, 1.6 times larger chromophore maturation rate, and 2.0 times higher photostability under 440–480 nm mercury arc light illumination. The applicability of Gamillus as a molecular tag was demonstrated by acquiring the correct localization

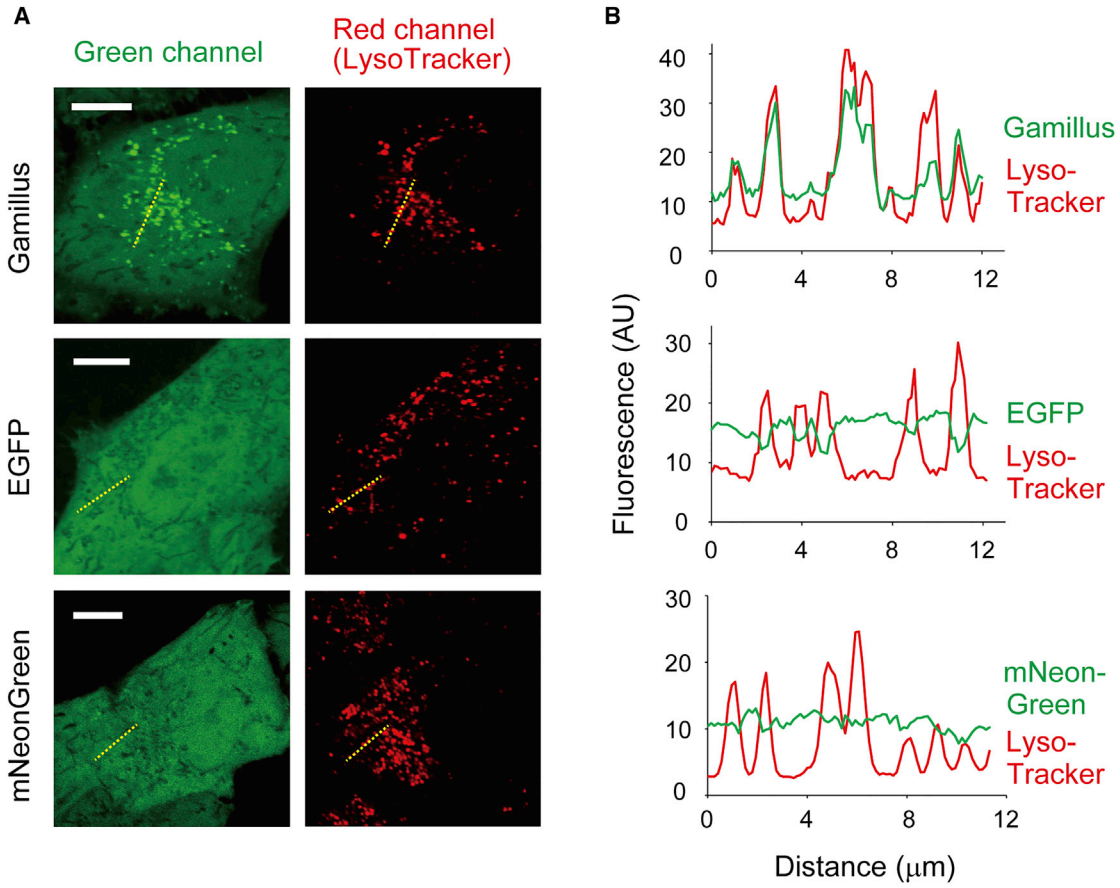

Figure 6. Fluorescence Accumulation in Lysosomes by Macroautophagy

(A) Confocal images of HeLa cells expressing non-fused Gamillus, EGFP, or mNeonGreen after incubation with LysoTracker red. Images were taken 3 days after transfection. Scale bars, 10 μm.

(B) Line profiles of fluorescence intensity on the yellow dots shown in (A).

See also Figure S7.

pattern of Gamillus fusions in a variety of cellular structures including ones difficult to target (e.g., β-tubulin and H2B), and subcellular compartments including acidic organelles (e.g., lysosomes and secretory granules). Applicability of Gamillus to imaging in acidic conditions was revealed through tracking of autophagy-mediated molecular migration to lysosomes. Gamillus can assist acquisition of multidimensional data in multicolor fluorescent imaging of the acidic environment that was not possible with the previously available fluorescent proteins and contribute to unveiling the mechanisms of hitherto untouched physiological functions.

STAR★METHODS

Detailed methods are provided in the online version of this paper and include the following:

- KEY RESOURCES TABLE
- CONTACT FOR REAGENT AND RESOURCE SHARING
- EXPERIMENTAL MODEL AND SUBJECT DETAILS
  - Preparation of HeLa Cells
- METHODS DETAILS
  - General Gene Construction Method
  - cDNA Cloning from *Olindias formosa*
  - Phylogenetic Analysis
  - Protein 3D Structure Modeling
  - Mutagenesis and Screening of Libraries
  - Protein Expression and Purification
  - Spectral Measurement
  - Molar Extinction Coefficient (ε) and Fluorescence Quantum Yield (Φ) Determination
  - Size-Exclusion Chromatography
  - Chromophore Maturation Speed Measurement
  - Mature Fraction Measurement
  - pH Sensitivity Measurement and pK_a Determination
  - *In Vitro* Stability Measurement
  - X-Ray Crystallography
  - Mammalian Expression Vector
  - Microscopy
  - Photochromic Behavior
  - Photobleaching Measurement
  - OSER Assay
  - Cytotoxicity Measurement

SUPPLEMENTAL INFORMATION

Supplemental Information includes seven figures, three tables, and one movie and can be found with this article online at https://doi.org/10.1016/j.chembiol.2017.12.005.

ACKNOWLEDGMENTS

We thank Kazuya Okuizumi (Kamo Aquarium, Japan) for kindly providing us flower hat jellyfishes, *Olindias formosa*. This work was performed using a synchrotron beamline BL44XU at SPring-8 under the Cooperative Research Program of the Institute for Protein Research, Osaka University. Diffraction data were collected at the Osaka University beamline BL44XU at SPring-8 (Harima, Japan) under proposal numbers 2016A6627 and 2016B6627. We thank Matthew J Daniels for critical reading of the manuscript. This work was supported by the 'CREST, JST' (No. JPMJCR15N3, JPMJCR12M6), 'Health Labor Sciences Research grant', the JSPS 'Grant-in-Aid for Young Scientists (A)' (No. 18687014), and the MEXT 'Grant-in-Aid for Scientific Research on Innovative Areas' 'Spying minority in biological phenomena' (No. JP23115003) to T.N., and 'Interplay of developmental clock and extracellular environment in brain formation' (No. JP16H06487) to T.M. The authors have filed an international patent application for Gamillus (no. PCT-JP2017-009759).

AUTHOR CONTRIBUTIONS

Conceptualization, T.N.; Methodology, H.S., R.N., T.M., and T.N.; Validation, H.S.; Formal Analysis, H.S., R.N., K.S., and T.M.; Investigation, H.S., Y.M., R.N., and T.M.; Resources, R.N., T.M., and T.N.; Writing – Original Draft, H.S. and T.M.; Writing – Review & Editing, H.S., Y.M., R.N., T.M., and T.N.; Visualization, H.S., R.N., and T.M.; Supervision, T.M. and T.N.; Funding Acquisition, R.N., T.M., and T.N.

Received: July 19, 2017
Revised: October 20, 2017
Accepted: December 5, 2017
Published: December 28, 2017

REFERENCES

Adams, P.D., Afonine, P.V., Bunkóczi, G., Chen, V.B., Davis, I.W., Echols, N., Headd, J.J., Hung, L.W., Kapral, G.J., Grosse-Kunstleve, R.W., et al. (2010). PHENIX: a comprehensive Python-based system for macromolecular structure solution. Acta Crystallogr. D Biol. Crystallogr. *66*, 213–221.

Ai, H.W., Baird, M.A., Shen, Y., Davidson, M.W., and Campbell, R.E. (2014). Engineering and characterizing monomeric fluorescent proteins for live-cell imaging applications. Nat. Protoc. *9*, 910–928.

Altschul, S.F., Madden, T.L., Schäffer, A.A., Zhang, J., Zhang, Z., Miller, W., and Lipman, D.J. (1997). Gapped BLAST and PSI-BLAST: a new generation of protein database search programs. Nucleic Acids Res. *25*, 3389–3402.

Ando, R., Mizuno, H., and Miyawaki, A. (2004). Regulated fast nucleocytoplasmic shuttling observed by reversible protein highlighting. Science *306*, 1370–1373.

Bizzarri, R., Serresi, M., Cardarelli, F., Abbruzzetti, S., Campanini, B., Viappiani, C., and Beltram, F. (2010). Single amino acid replacement makes *Aequorea victoria* fluorescent proteins reversibly photoswitchable. J. Am. Chem. Soc. *132*, 85–95.

Bomati, E.K., Haley, J.E., Noel, J.P., and Deheyn, D.D. (2014). Spectral and structural comparison between bright and dim green fluorescent proteins in *Amphioxus*. Sci. Rep. *4*, 5469.

Bordoli, L., Kiefer, F., Arnold, K., Benkert, P., Battey, J., and Schwede, T. (2009). Protein structure homology modeling using SWISS-MODEL workspace. Nat. Protoc. *4*, 1–13.

Boya, P., and Kroemer, G. (2008). Lysosomal membrane permeabilization in cell death. Oncogene *27*, 6434–6451.

Campbell, R.E., Tour, O., Palmer, A.E., Steinbach, P.A., Baird, G.S., Zacharias, D.A., and Tsien, R.Y. (2002). A monomeric red fluorescent protein. Proc. Natl. Acad. Sci. USA *99*, 7877–7882.

Casey, J.R., Grinstein, S., and Orlowski, J. (2010). Sensors and regulators of intracellular pH. Nat. Rev. Mol. Cell Biol. *11*, 50–61.

Christensen, K.A., Myers, J.T., and Swanson, J.A. (2002). pH-dependent regulation of lysosomal calcium in macrophages. J. Cell Sci. *115*, 599–607.

Chu, J., Oh, Y., Sens, A., Ataie, N., Dana, H., Macklin, J.J., Laviv, T., Welf, E.S., Dean, K.M., Zhang, F., et al. (2016). A bright cyan-excitable orange fluorescent protein facilitates dual-emission microscopy and enhances bioluminescence imaging in vivo. Nat. Biotechnol. *34*, 760–767.

Collaborative Computational Project, Number 4 (1994). The CCP4 suite: programs for protein crystallography. Acta Crystallogr. D Biol. Crystallogr. *50*, 760–763.

Costantini, L.M., Fossati, M., Francolini, M., and Snapp, E.L. (2012). Assessing the tendency of fluorescent proteins to oligomerize under physiologic conditions. Traffic *13*, 643–649.

Cranfill, P.J., Sell, B.R., Baird, M.A., Allen, J.R., Lavagnino, Z., de Gruiter, H.M., Kremers, G.J., Davidson, M.W., Ustione, A., and Piston, D.W. (2016). Quantitative assessment of fluorescent proteins. Nat. Methods *13*, 557–562.

Emsley, P., and Cowtan, K. (2004). Coot: model-building tools for molecular graphics. Acta Crystallogr. D Biol. Crystallogr. *60*, 2126–2132.

Evdokimov, A.G., Pokross, M.E., Egorov, N.S., Zaraisky, A.G., Yampolsky, I.V., Merzlyak, E.M., Shkoporov, A.N., Sander, I., Lukyanov, K.A., and Chudakov, D.M. (2006). Structural basis for the fast maturation of Arthropoda green fluorescent protein. EMBO Rep. *7*, 1006–1012.

Gasteiger, E., Hoogland, C., Gattiker, A., Duvaud, S., Wilkins, M.R., Appel, R.D., and Bairoch, A. (2005). The Proteomics Protocols Handbook (Humana Press).

Goedhart, J., von Stetten, D., Noirclerc-Savoye, M., Lelimousin, M., Joosen, L., Hink, M.A., van Weeren, L., Gadella, T.W., Jr., and Royant, A. (2012). Structure-guided evolution of cyan fluorescent proteins towards a quantum yield of 93%. Nat. Commun. *3*, 751.

Griesbeck, O., Baird, G.S., Campbell, R.E., Zacharias, D.A., and Tsien, R.Y. (2001). Reducing the environmental sensitivity of yellow fluorescent protein. Mechanism and applications. J. Biol. Chem. *276*, 29188–29194.

Gross, L.A., Baird, G.S., Hoffman, R.C., Baldridge, K.K., and Tsien, R.Y. (2000). The structure of the chromophore within DsRed, a red fluorescent protein from coral. Proc. Natl. Acad. Sci. USA *97*, 11990–11995.

Higgins, D.G., Thompson, J.D., and Gibson, T.J. (1996). Using CLUSTAL for multiple sequence alignments. Methods Enzymol. *266*, 383–402.

Hoi, H., Howe, E.S., Ding, Y., Zhang, W., Baird, M.A., Sell, B.R., Allen, J.R., Davidson, M.W., and Campbell, R.E. (2013). An engineered monomeric *Zoanthus* sp. yellow fluorescent protein. Chem. Biol. *20*, 1296–1304.

Hunt, M.E., Modi, C.K., Aglyamova, G.V., Ravikant, D.V., Meyer, E., and Matz, M.V. (2012). Multi-domain GFP-like proteins from two species of marine hydrozoans. Photochem. Photobiol. Sci. *11*, 637–644.

Huotari, J., and Helenius, A. (2011). Endosome maturation. EMBO J. *30*, 3481–3500.

Katayama, H., Yamamoto, A., Mizushima, N., Yoshimori, T., and Miyawaki, A. (2008). GFP-like proteins stably accumulate in lysosomes. Cell Struct. Funct. *33*, 1–12.

Kimura, S., Noda, T., and Yoshimori, T. (2007). Dissection of the autophagosome maturation process by a novel reporter protein, tandem fluorescent-tagged LC3. Autophagy *3*, 452–460.

Lawrence, M.S., Phillips, K.J., and Liu, D.R. (2007). Supercharging proteins can impart unusual resilience. J. Am. Chem. Soc. *129*, 10110–10112.

Lukyanov, K., Diatchenko, L., Chenchik, A., Nanisetti, A., Siebert, P., Usman, N., Matz, M., and Lukyanov, S. (1997). Construction of cDNA libraries from small amounts of total RNA using the suppression PCR effect. Biochem. Biophys. Res. Commun. *230*, 285–288.

Martinez-Arca, S., Rudge, R., Vacca, M., Raposo, G., Camonis, J., Proux-Gillardeaux, V., Daviet, L., Formstecher, E., Hamburger, A., Filippini, F., et al. (2003). A dual mechanism controlling the localization and function of exocytic v-SNAREs. Proc. Natl. Acad. Sci. USA *100*, 9011–9016.

Masuda, H., Takenaka, Y., Yamaguchi, A., Nishikawa, S., and Mizuno, H. (2006). A novel yellowish-green fluorescent protein from the marine copepod, *Chiridius poppei*, and its use as a reporter protein in HeLa cells. Gene *372*, 18–25.

Matsuda, T., Miyawaki, A., and Nagai, T. (2008). Direct measurement of protein dynamics inside cells using a rationally designed photoconvertible protein. Nat. Methods *5*, 339–345.

Matz, M., Shagin, D., Bogdanova, E., Britanova, O., Lukyanov, S., Diatchenko, L., and Chenchik, A. (1999). Amplification of cDNA ends based on template-switching effect and step-out PCR. Nucleic Acids Res. *27*, 1558–1560.

Merzlyak, E.M., Goedhart, J., Shcherbo, D., Bulina, M.E., Shcheglov, A.S., Fradkov, A.F., Gaintzeva, A., Lukyanov, K.A., Lukyanov, S., Gadella, T.W., et al. (2007). Bright monomeric red fluorescent protein with an extended fluorescence lifetime. Nat. Methods *4*, 555–557.

Mindell, J.A. (2012). Lysosomal acidification mechanisms. Annu. Rev. Physiol. *74*, 69–86.

Murshudov, G.N., Vagin, A.A., and Dodson, E.J. (1997). Refinement of macromolecular structures by the maximum-likelihood method. Acta Crystallogr. D Biol. Crystallogr. *53*, 240–255.

Otwinowski, Z., and Minor, W. (1997). Processing of X-ray diffraction data collected in oscillation mode. Methods Enzymol. *276*, 307–326.

Pettersen, E.F., Goddard, T.D., Huang, C.C., Couch, G.S., Greenblatt, D.M., Meng, E.C., and Ferrin, T.E. (2004). UCSF Chimera—a visualization system for exploratory research and analysis. J. Comput. Chem. *25*, 1605–1612.

Roberts, T.M., Rudolf, F., Meyer, A., Pellaux, R., Whitehead, E., Panke, S., and Held, M. (2016). Identification and characterisation of a pH-stable GFP. Sci. Rep. *6*, 28166.

Rost, B.R., Schneider, F., Grauel, M.K., Wozny, C., Bentz, C.G., Blessing, A., Rosenmund, T., Jentsch, T.J., Schmitz, D., Hegemann, P., et al. (2015). Optogenetic acidification of synaptic vesicles and lysosomes. Nat. Neurosci. *18*, 1845–1852.

Saito, K., Chang, Y.F., Horikawa, K., Hatsugai, N., Higuchi, Y., Hashida, M., Yoshida, Y., Matsuda, T., Arai, Y., and Nagai, T. (2012). Luminescent proteins for high-speed single-cell and whole-body imaging. Nat. Commun. *3*, 1262.

Sawano, A., and Miyawaki, A. (2000). Directed evolution of green fluorescent protein by a new versatile PCR strategy for site-directed and semi-random mutagenesis. Nucleic Acids Res. *28*, E78.

Schneider, C.A., Rasband, W.S., and Eliceiri, K.W. (2012). NIH Image to ImageJ: 25 years of image analysis. Nat. Methods *9*, 671–675.

Settembre, C., Fraldi, A., Medina, D.L., and Ballabio, A. (2013). Signals from the lysosome: a control centre for cellular clearance and energy metabolism. Nat. Rev. Mol. Cell Biol. *14*, 283–296.

Shagin, D.A., Barsova, E.V., Yanushevich, Y.G., Fradkov, A.F., Lukyanov, K.A., Labas, Y.A., Semenova, T.N., Ugalde, J.A., Meyers, A., Nunez, J.M., et al. (2004). GFP-like proteins as ubiquitous metazoan superfamily: evolution of functional features and structural complexity. Mol. Biol. Evol. *21*, 841–850.

Shaner, N.C., Lambert, G.G., Chammas, A., Ni, Y., Cranfill, P.J., Baird, M.A., Sell, B.R., Allen, J.R., Day, R.N., Israelsson, M., et al. (2013). A bright monomeric green fluorescent protein derived from *Branchiostoma lanceolatum*. Nat. Methods *10*, 407–409.

Shimomura, O., Johnson, F.H., and Saiga, Y. (1962). Extraction, purification and properties of aequorin, a bioluminescent protein from the luminous hydromedusan, *Aequorea*. J. Cell. Comp. Physiol. *59*, 223–239.

Suzuki, K., Kimura, T., Shinoda, H., Bai, G., Daniels, M.J., Arai, Y., Nakano, M., and Nagai, T. (2016). Five colour variants of bright luminescent protein for real-time multicolour bioimaging. Nat. Commun. *7*, 13718.

Takemoto, K., Matsuda, T., Sakai, N., Fu, D., Noda, M., Uchiyama, S., Kotera, I., Arai, Y., Horiuchi, M., Fukui, K., et al. (2013). SuperNova, a monomeric photosensitizing fluorescent protein for chromophore-assisted light inactivation. Sci. Rep. *3*, 2629.

Tiwari, D.K., Arai, Y., Yamanaka, M., Matsuda, T., Agetsuma, M., Nakano, M., Fujita, K., and Nagai, T. (2015). A fast- and positively photoswitchable fluorescent protein for ultralow-laser-power RESOLFT nanoscopy. Nat. Methods *12*, 515–518.

Tomosugi, W., Matsuda, T., Tani, T., Nemoto, T., Kotera, I., Saito, K., Horikawa, K., and Nagai, T. (2009). An ultramarine fluorescent protein with increased photostability and pH insensitivity. Nat. Methods *6*, 351–353.

Tsien, R.Y. (1998). The green fluorescent protein. Annu. Rev. Biochem. *67*, 509–544.

Vagin, A., and Teplyakov, A. (1997). MOLREP: an automated program for molecular replacement. J. Appl. Crystallogr. *30*, 1022–1025.

Yanushevich, Y.G., Staroverov, D.B., Savitsky, A.P., Fradkov, A.F., Gurskaya, N.G., Bulina, M.E., Lukyanov, K.A., and Lukyanov, S.A. (2002). A strategy for the generation of non-aggregating mutants of Anthozoa fluorescent proteins. FEBS Lett. *511*, 11–14.

Zhao, Y., Araki, S., Wu, J., Teramoto, T., Chang, Y.F., Nakano, M., Abdelfattah, A.S., Fujiwara, M., Ishihara, T., Nagai, T., et al. (2011). An expanded palette of genetically encoded Ca^{2+} indicators. Science *333*, 1888–1891.

Zhu, Y.Y., Machleder, E.M., Chenchik, A., Li, R., and Siebert, P.D. (2001). Reverse transcriptase template switching: a SMART approach for full-length cDNA library construction. Biotechniques *30*, 892–897.

STAR★METHODS

KEY RESOURCES TABLE

REAGENT or RESOURCE	SOURCE	IDENTIFIER
Bacterial and Virus Strains		
Escherichia coli strain XL10-Gold	Agilent Technologies	Cat#200314
Escherichia coli strain JM109(DE3)	Promega	Cat#P9801
Escherichia coli strain XL-1	Agilent Technologies	Cat#200236
Escherichia coli strain B834(DE3)	Novagen	Cat#69041
Critical Commercial Assays		
KOD Plus DNA polymerase	Toyobo Life Sciences	Cat#KOD-201
rTaq DNA polymerase	Toyobo Life Sciences	Cat#TAP-201
*Bam*HI	Takara	Cat#1010A
*Pst*I	NEB	Cat#R0140S
*Eco*RI	Takara	Cat#1040A
*Xho*I	Takara	Cat#1094A
*Kpn*I	Takara	Cat#1068A
*Hind*III	Takara	Cat#1060A
*Sal*I	Takara	Cat#1080A
*Not*I	Takara	Cat#1166A
*Bgl*II	Takara	Cat#1021A
*Age*I	Nippon Gene	Cat#313-02561
QIAEX II gel extraction kit	Qiagen	Cat#20051
T4 ligase	Promega	Cat#M1804
Pfu polymerase	Agilent Technologies	Cat#600154
Pfu ligase	Agilent Technologies	Cat#600191
BigDye Terminator v1.1 Cycle Sequence Kit	ThermoFisher Scientific	Cat#4337450
RNA aqueous kit	Ambion	Cat#AM1912
SMARTScribe reverse transcriptase	Clontech	Cat#639523
Advantage 2 DNA polymerase buffer & DNA polymerase	Clontech	Cat#639201
Ni-NTA Agarose	Qiagen	Cat#30230
AnaeroPack	Mitsubishi Gas	Cat#A-07
SeMet core medium	Wako	Cat#391-01541
Seleno-L-Methionine	Nacalai tesque	Cat#02286-46
Vitamin	Sigma-Aldrich	Cat#K3129
Dulbecco's modified Eagle's medium	Sigma-Aldrich	Cat#D6046
fetal bovine serum	Biowest	Cat#S14198S1780
DMEM/F12	ThermoFisher Scientific	Cat#11039-021
penicillin/streptomycin	ThermoFisher Scientific	Cat#15140
Lipofectamine 2000	Invitrogen	Cat#11668-019
LysoTracker Red DND-99	Invitrogen	Cat#L7528
Deposited Data		
DNA sequence of dfGFP	This paper	DDBJ ID: LC309248
DNA sequence of Gamillus (codon optimized for human expression)	This paper	DDBJ ID: LC309249
Structure of Gamillus (fluorescence state)	This paper	pdb: 5Y00 https://pdbj.org/status-search?pdbid=5y00
Structure of Gamillus (non-fluorescence state)	This paper	pdb: 5Y01 https://pdbj.org/status-search?pdbid=5y01

(*Continued on next page*)

Continued

REAGENT or RESOURCE	SOURCE	IDENTIFIER
Experimental Models: Cell Lines		
HeLa	RIKEN BRC	N/A
Oligonucleotides		
Primer sequences are provided in Table S3	This paper	N/A
Synthetic cDNA: CpYGFP	(Masuda et al., 2006)	GeneArt Strings DNA Fragments https://www.thermofisher.com/jp/en/home/life-science/cloning/gene-synthesis/gene-strings-dna-fragments.html
Synthetic cDNA: Gamillus (codon optimized for human expression)	This paper	Same as above
Recombinant DNA		
Plasmid: Gamillus-pRSET$_B$	This paper	N/A
Plasmid: mNeonGreen	(Shaner et al., 2013)	Allele Biotechnology
Plasmid: bfloGFPa1-pPET24(+)	(Bomati et al., 2014)	A gift from Dimitri D Deheyn
Plasmid: pH-tdGFP-pFA6a	(Roberts et al., 2016)	Addgene Plasmid #74322
Plasmid: pCMV-lyso-pHluorin	(Rost et al., 2015)	Addgene Plasmid #70113
Plasmid: pmRFP-LC3	(Kimura et al., 2007)	Addgene Plasmid #21075
Plasmid: pEGFP-VAMP2	(Martinez-Arca et al., 2003)	Addgene Plasmid #42308
Plasmid: pCytERM_mScarlet_N1	(Costantini et al., 2012)	Addgene Plasmid #85066
Plasmid: pcDNA3-CoxVIII×2-Nano-lantern	(Saito et al., 2012)	N/A
Plasmid: pcDNA3-Nano-lantern-H2B	(Saito et al., 2012)	N/A
Plasmid: pcDNA3-lyn-Phamlet	(Matsuda et al., 2008)	N/A
Plasmid: pcDNA3-Golgi-Phamret	(Matsuda et al., 2008)	N/A
Plasmid: pcDNA3-paxillin-Kohinoor	(Tiwari et al., 2015)	N/A
Plasmid: pcDNA3-zyxin-Kohinoor	(Tiwari et al., 2015)	N/A
Plasmid: pcDNA3-Kohinoor-β-actin	(Tiwari et al., 2015)	N/A
Plasmid: pEGFP-N1-β-tubulin-Kohinoor	(Tiwari et al., 2015)	N/A
Plasmid: pcDNA3-Kohinoor-fibrillarin	(Tiwari et al., 2015)	N/A
Plasmid: pcDNA3-LAMP1-eNano-lantern	(Suzuki et al., 2016)	N/A
Plasmid: pNCS-mNeonGreen	(Shaner et al., 2013)	Allele Biotechnology http://www.allelebiotech.com/mneongreen/
Software and Algorithms		
BLAST	(Altschul et al., 1997)	https://blast.ncbi.nlm.nih.gov/Blast.cgi
ClustalW	(Higgins et al., 1996)	http://www.genome.jp/tools-bin/clustalw
GENETYX version 12	Genetyx	https://www.genetyx.co.jp/products/genetyx_12/index.html
SWISS-MODEL	(Bordoli et al., 2009)	https://swissmodel.expasy.org/
UCSF chimera	(Pettersen et al., 2004)	https://www.cgl.ucsf.edu/chimera/download.html
Origin8	OriginLab	http://www.originlab.com/
ProtParam	(Gasteiger et al., 2005)	http://web.expasy.org/protparam/
HKL2000 program package	(Otwinowski and Minor, 1997)	http://www.hkl-xray.com/
AutoSol (PHENIX program suite)	(Adams et al., 2010)	https://www.phenix-online.org/
MOLREP, COOT, REFMAC (CCP4 program)	(Collaborative Computational Project, Number 4, 1994) (Vagin and Teplyakov, 1997) (Emsley and Cowtan, 2004) (Murshudov et al., 1997)	http://www.ccp4.ac.uk/
PyMOL	PyMOL Molecular Graphics System	https://www.pymol.org/
MetaMorph	Molecular Devices	http://www.nihonmdc.com/pages/UIC/MetaImaging_MetaMorph.html
ImageJ (FIJI)	(Schneider et al., 2012)	http://imagej.net/Fiji/Downloads

CONTACT FOR REAGENT AND RESOURCE SHARING

Further information and requests for resources and reagents should be directed to and will be fulfilled by the Lead Contact, Takeharu Nagai (ng1@sanken.osaka-u.ac.jp).

EXPERIMENTAL MODEL AND SUBJECT DETAILS

Preparation of HeLa Cells

HeLa cells (RIKEN BRC) were cultured in Dulbecco's modified Eagle's medium (DMEM) (D6046, Sigma-Aldrich) supplemented with 10% fetal bovine serum (FBS) (S14198S1780, Biowest) at 37°C with 5% CO_2 supply. For imaging, the cells were prepared in 35 mm collagen-coated (Cellmatrix Type I-C, Nitta Gelatin) handmade glass-bottom dishes. The cells were transfected with 2.0 μg of DNA plasmids using the calcium phosphate method. The cells were incubated with the DNA mixture for 12 h, washed with PBS, and incubated in fresh DMEM with 10% FBS. Phenol red-free DMEM/F12 (11039-021, ThermoFisher Scientific) supplemented with 1% penicillin/streptomycin (15140, ThermoFisher Scientific) was used as imaging medium.

METHODS DETAILS

General Gene Construction Method

Synthetic DNA oligonucleotides used for gene construction were purchased from Hokkaido system science. For gene construction, KOD Plus and rTaq DNA polymerase (Toyobo Life Sciences) were used for regular PCR and error-prone PCR respectively (Griesbeck et al., 2001). PCR products were treated with phenol/chloroform followed by ethanol precipitation, and digested by restriction enzymes (Takara or New England Biolabs) according to the manufacturers' recommended protocols. The products of restriction digests were purified by agarose gel electrophoresis followed by DNA isolation using a QIAEX II gel extraction kit (Qiagen). Ligation was performed by using T4 ligase (Promega). The QuikChange method was applied for site-specific mutagenesis (Sawano and Miyawaki, 2000). Pfu polymerase (BioAcademia) and Pfu ligase (Agilent Technologies) were used to create mutated, circular single-strand DNA. The cDNA sequences were confirmed by dye terminator cycle sequencing using the BigDye Terminator v1.1 Cycle Sequence Kit (Thermo Fisher Scientific). Small-scale plasmid DNA preparation was performed using alkaline lysis methods on bacteria collected from 1.5 ml LB cultures, followed by ethanol precipitation. Large-scale plasmid DNA preparation was performed by alkaline lysis methods using bacteria collected from 200 ml LB cultures, followed by isopropanol precipitation, PEG 8000 precipitation, and phenol/chloroform extraction.

cDNA Cloning from *Olindias formosa*

Flower hat jellyfish were provided by Kamo Aquarium (Tsuruoka, Japan). About 500 mg of the frozen jellyfish samples from fluorescent tentacles was ground and placed in 1.5 ml of RNAlater solution (Ambion). The total RNA was extracted using the RNA aqueous kit (Ambion, AM1912) following the manufacture's protocol. The quality and integrity of the extracted total RNA was assessed by agarose gel electrophoresis, where the 28S and 18S rRNA bands were observed, and 200–1000 ng of extracted total RNA was used to synthesize the first strand of cDNA. Oligo T primer was added to a final concentration of 15 μM and incubated at 65°C for 3 min, with 1 min on ice to initialize the binding of oligo T primer to the poly-A tail of mRNA. A second solution containing 2 μl of 5× first strand buffer, 1 μl of DTT, 1 μl of 10 μM oligo G primer, and 1 μl of SMARTScribe reverse transcriptase (Clontech, 639523) was added. The first strand of cDNA was synthesized by incubating at 42°C for 1 h, followed by a 15 min 65°C incubation to deactivate the reverse transcriptase. Note that the Oligo G primer was ligated to the 5' end of the newly synthesized cDNA strand using the template switching effect of the Moloney murine leukemiavirus reverse transcriptase (Matz et al., 1999; Zhu et al., 2001). The obtained first stand of the cDNA library was further amplified by PCR. The inverted terminal repeats in the cap and Step-Out cap primers allowed for suppression of unwanted PCR products due to the nonspecific binding of Oligo G and Oligo T (Lukyanov et al., 1997). The addition of base A and AA at the 3-prime end of the Step-Out cap primer was used to account for the frame shift in the open reading frame. The PCR reaction was performed as follows. The cDNA sample was mixed with 23.7 μl of dH_2O, 3 μl of Advantage 2 DNA polymerase buffer (Clontech 639201), 0.6 μl of 10 mM dNTPs, 0.6 μl of Advantage 2 DNA polymerase (Clontech 639201), and 0.6 μl of 10 μM Cap primer (or 0.6 μl of 15 μM Step-Out Cap primer). The cDNA library was amplified using the following PCR procedure: 94°C for 5 min, 94°C for 40 s, 60°C for 1 min, 72°C for 5 min, and step 2 to 4 were repeated for a varying number of cycles depending on the sample quality. In general, the number of PCR cycles was kept minimal to avoid over amplification of non-specific cDNA fragments. The amplified cDNA library with different open reading frames was purified using the QIAquick PCR purification kit (Qiagen), and ~120 ng of DNA was used to ligate into 50 ng of PGEM-T vector in a 10 μl reaction volume, and 3 μl of the ligation product was transformed into 50 μl of XL-I blue super competent cells. The transformed cells were cultured on LB agar plates containing 0.1 mg/ml ampicillin and 0.5 mM IPTG at 37°C for 12 h, followed by incubation at room temperature for another 24 h. The resultant colonies were screened for fluorescence under blue light excitation and different emission filter sets. The identified fluorescent colonies were subcultured and the DNA was extracted and sequenced.

Phylogenetic Analysis

The amino acid identity and similarity of dfGFP was assessed using the BLAST server (Altschul et al., 1997) (https://blast.ncbi.nlm.nih.gov/Blast.cgi). The sequence was aligned with hydrozoan FP sequences using the ClustalW online server (Higgins et al., 1996), and the phylogenetic tree and sequence alignment graphics were generated using GENETYX version 12 software (Genetyx). The GenBank accession number for the aligned FPs are as follows: avGFP (P42212), anm2CP (AY485336), Ember_a-d (HQ699262), anm1GFP1 (AY485334), anm1GFP2 (AY485335), phiYFP (AY485333), amagGFP509 (ACC54354), amacGFP (AF435432), acoeGFP (AY151052), abeGFP_a-b (HQ699261), clytiaGFP (2HPW_A), obeCFP (JN385282), obeGFP (JN385283), and obeYFP (JN385284).

Protein 3D Structure Modeling

Homology model structures of dfGFP, Gamillus0.4, and Gamillus0.5 were built from their amino acid sequences using the SWISS-MODEL server (https://swissmodel.expasy.org/). The models were superimposed onto a published crystal structure of the KillerRed dimer (pdb: 3gb3) using UCSF chimera software to predict the dimer interface of dfGFP.

Mutagenesis and Screening of Libraries

For bacterial expression, DNA sequences of the FPs were amplified by PCR, digested with *Bam*HI (or *Pst*I) and *Eco*RI, and subcloned into the bacterial expression vector, $pRSET_B$. The constructed expression vectors were transformed into *Escherichia coli* XL10-Gold and cultured in 1.5 ml LB media supplemented with 0.1 mg/ml carbenicillin. Site-specific mutations were introduced into dfGFP sequences using the QuikChange method. To create a bacterial library of mutated dfGFP, random mutations were introduced into the gene fragments by error-prone PCR, and ligated into a $pRSET_B$ vector that was transformed into *E. coli* JM109(DE3). The bacteria were grown on LB agar plates with 0.1 mg/ml carbenicillin at 37°C overnight (or additional incubation at room temperature for 1 day). For each round, ~15,000 colonies were prepared and screened by eye for fluorescence under blue-light illumination (Safe Imager Transluminator, S37102, Invitrogen), or screened using a custom-made illumination system equipped with a charge-coupled device (CCD) camera (QIClick, QImaging), a LED light source (Spectra X Light Engine, Lumencor), a 475/28 nm excitation bandpass filter (Semrock), a 520–20 nm emission bandpass filter (Asahi Spectra), and an integrating sphere (RTC-060-SF, Labsphere) for homogeneous illumination. The data were analyzed by ImageJ software (Schneider et al., 2012). Screened colonies were cultured in LB media with 0.1 mg/ml carbenicillin, and the lysates were used to check the pH dependency. After improvement of Gamillus, we designed and purchased the synthetic DNA encoding codon-optimized Gamillus for human expression from Life Technologies (GeneArt Strings DNA Fragments). The gene encoding Gamillus was inserted into a $pRSET_B$ vector (Invitrogen) or pcDNA3 vector at *Bam*HI and *Eco*RI sites respectively. EGFP, mNeonGreen (Shaner et al., 2013), CpYGFP (Masuda et al., 2006), bfloGFPa1 (Bomati et al., 2014) and pH-tdGFP (Roberts et al., 2016) sequences were also inserted in a $pRSET_B$ or pcDNA3 vector at *Bam*HI and *Eco*RI sites.

Protein Expression and Purification

FPs were expressed in *E. coli* JM109(DE3) and cultured at 23°C for 72 h in LB medium supplemented with 0.1 mg/ml carbenicillin. The bacteria were collected, suspended in PBS buffer, and homogenized by pressure using a FRENCH Press (Thermo Fisher Scientific). FPs were purified from the supernatant using Ni-NTA Agarose (Qiagen), followed by buffer-exchange to 20 mM HEPES (pH = 7.4) using a PD10 column (GE Healthcare).

Spectral Measurement

For absorption spectra measurements, FPs were diluted in 20 mM HEPES buffer (pH 7.4) or trisodium citrate/borate buffer, and recorded by a spectrophotometer (V-630 BIO, Jasco). For excitation and emission spectra measurements, FPs were diluted in the buffer until absorbance at the measured wavelength reaches less than 0.05 in order to prevent reabsorption of the emitted light. Excitation and emission spectra were recorded using a fluorescence spectrometer (F-7000, Hitachi).

Molar Extinction Coefficient (ε) and Fluorescence Quantum Yield (Φ) Determination

The ε of the FPs was calculated by using the protein concentration determined using the following alkali-denaturation methods (Gross et al., 2000; Shaner et al., 2013). FPs were prepared in 20 mM HEPES (pH 7.4) buffer and absorption spectra were recorded to determine the peak absorption value ($A_{peak\cdot FP}$). FPs prepared in the same buffer were denatured by mixing with an equal amount of 2.0 M NaOH, and the absorption spectra were recorded immediately to determine the peak absorption value at around ~447 nm ($A_{447nm\cdot denatured}$). By assuming that denatured chromophores have an ε equivalent to that of avGFP (44,000 $M^{-1}cm^{-1}$), we determined the ε as ($A_{peak\cdot FP}/A_{447nm\cdot denatured}$) × 44,000 $M^{-1}cm^{-1}$. The absolute fluorescence quantum yield was determined by integrating the sphere measurement (Absolute PL quantum yield spectrometer, C11347, Hamamatsu). For the measurement, FPs were diluted with buffer until the absorbance at excitation wavelength reached 0.05.

Size-Exclusion Chromatography

Size-exclusion chromatography was performed using an ÄKTA explorer 10S equipped with a Superdex 200 10/300 GL column (GE Healthcare), where 500 μl of purified FPs were loaded on the column after dilution in 20 mM HEPES (pH 7.4) containing 150 mM NaCl to the desired concentration and filtration through a 0.20 μm pore filter (Millipore). The same buffer was used for the mobile phase at a flow rate of 0.75 ml/min. Absorption was measured at the wavelength of the absorption spectrum peak.

Chromophore Maturation Speed Measurement

For measurement of the oxygen-dependent chromophore maturation speed, FPs were expressed in the *E. coli* JM109(DE3). The 10 ml LB media culture supplemented with 0.1 mg/ml carbenicillin was grown at 37°C for 1–1.5 days in 50 mL bioreactor tubes (87050, BMBio). Tubes were packed in a tightly sealed plastic bag with an AnaeroPack (Mitsubishi Gas) that absorbs O_2 and generates CO_2 in order to achieve anaerobic conditions. Before exposing to air, it was confirmed that there was little fluorescence in the liquid cultures. After chilling the cultures on ice, the FPs were extracted by sonication and clarified by centrifugation. The extract was incubated at 37°C with exposure to air, and the emission was recorded by a Spectrofluorometer (FP-750, Jasco) until the fluorescence signal reached a plateau. The chromophore maturation halftime for the FPs was calculated by fitting the data to a single exponential growth function using Origin8 software (OriginLab).

Mature Fraction Measurement

The mature fraction was calculated as the concentration of chromophore divided by the concentration of total protein as follows (Chu et al., 2016). The concentration of chromophore was determined using the alkali-denaturation method. The concentration of total protein was determined using absorbance at 280 nm, and the extinction coefficient at 280 nm was determined by the program ProtParam (Gasteiger et al., 2005) (http://web.expasy.org/protparam/).

pH Sensitivity Measurement and pK_a Determination

To evaluate the pH sensitivity of the FPs, we prepared pH buffer as follows (Zhao et al., 2011). A solution containing 30 mM trisodium citrate and 30 mM borate was adjusted to pH 11.0, and HCl was added dropwise to prepare pH buffer ranging from pH 2.5 to 11.0. The fluorescence spectra of the FPs in the pH buffer were measured using a fluorescence spectrometer (F-7000, Hitachi). Measured fluorescence intensities were plotted against pH. The pK_a was determined by fitting the data to the following generalized Henderson-Hasselbalch equation by using Origin8 software (OriginLab):

$$F = \frac{F_1}{1 + 10^{n_{H1}(pK_a - pH)}}$$

(F_1 is fluorescence intensity at the maximum plateau. n_{H1} is apparent hill coefficient.)

The fitting for CpYGFP was achieved by assuming two fluorescence states (F_1 and F_2 state) in the following equation:

$$F = \frac{F_1}{1 + 10^{n_{H1}(pK_{a1} - pH)} + 10^{(n_{H1}pK_{a1} + n_{H2}pK_{a2} - (n_{H1} + n_{H2})pH)}} + \frac{F_1}{1 + 10^{n_{H1}(-pK_{a1} + pH)} + 10^{n_{H2}(pK_{a2} - pH)}}$$

(F_1 and F_2 are fluorescence intensities at the top and middle plateau. n_{H1} and n_{H2} are apparent hill coefficients between the F_1 and F_2 state, and F_2 and non-fluorescence state, respectively. pK_{a1} and pK_{a2} are the acid dissociation constants between the F_1 and F_2 state, and F_2 and non-fluorescence state, respectively. The pK_a for CpYGFP was defined as the pH value at which the fluorescence intensity becomes its half-maximum value.)

In Vitro Stability Measurement

For stability measurements in acidic conditions, purified FPs were incubated in plastic cuvettes with trisodium citrate/borate buffer and kept in the dark. Absorption, excitation, and emission spectra were recorded using a fluorescence spectrometer (F-7000, Hitachi). For stability measurements of the purified FPs in guanidine chloride solution the fluorescence at 520 nm was recorded using a microplate reader (HS-9000, Corona) with 450 nm excitation in 20 s intervals.

X-Ray Crystallography

For preparation of selenomethionine (SeMet)-labeled Gamillus, the pRSET$_B$-Gamillus plasmid was transformed by electroporation into methionine auxotroph *E. coli* B834(DE3), and the bacterial colonies were cultured at 23°C for 72 h in 200 mL LeMaster medium made by mixing SeMet medium (Wako), 10 mg/ml glucose, 0.25 mg/ml $MgSO_4 \cdot H_2O$, 4.2 μg/ml $FeSO_4 \cdot H_2O$, 0.015 μg/ml H_2SO_4, 1/100 volume vitamin (K3129, Sigma-Aldrich), 50 μg/ml selenomethionine and 0.1 mg/ml carbenicillin (pH 7.5). Purification of the SeMet-labeled and native Gamillus was performed using a Ni-NTA column and a Superdex200 10/30 GL size-exclusion column (GE Healthcare), followed by concentration and buffer-exchange into 20 mM HEPES (pH 7.4) using a centrifugation column (Millipore). The crystallization condition for purified Gamillus was initially screened for by using a sitting-drop vapor diffusion method, and refined using a hanging-drop vapor diffusion method. The best crystals of SeMet-labeled and native Gamillus were obtained in buffer containing 1 M ammonium phosphate, 100 mM citrate-citric acid (pH 5.5) and 200 mM NaCl. The crystals were soaked with harvesting buffer containing 25% (v/v) glycerol for cryoprotection and flash frozen in liquid nitrogen. The diffraction data were collected using the BL44XU beamline at SPring-8 with an MX225-HE CCD detector (Rayonix) at 100 K. The diffraction data were processed and scaled with the HKL2000 program package (Otwinowski and Minor, 1997). The initial phase of Gamillus was determined by SAD phasing at 2.5 Å resolution. The selenium sites were located and the initial model was build using AutoSol in the PHENIX program suite (Adams et al., 2010) followed by phase extension up to 1.6 Å resolution using native data. The low pH state was first determined by molecular replacement with MOLREP (Vagin and Teplyakov, 1997) in the CCP4 program suite(Collaborative Computational Project, Number 4, 1994) using the atomic coordinates of the native structure as a search model. Model rebuilding

was performed manually using COOT (Emsley and Cowtan, 2004), and model refinement was performed using REFMAC (Murshudov et al., 1997). The quality of the diffraction data and the refinement statistics are listed in Table S2. Figures were prepared with PyMOL (The PyMOL Molecular Graphics System, Schrödinger, LLC.).

Mammalian Expression Vector

For cytosol expression, the PCR-amplified Gamillus sequence was inserted into the pcDNA3 mammalian expression vector at *Bam*HI and *Eco*RI restriction enzyme (RE) sites. For mitochondrial and nuclear expression, we replaced the Nano-lantern sequence with the Gamillus sequence in pcDNA3-CoxVIII×2-Nano-lantern (a duplicated mitochondrial localization sequence derived from the subunit-VIII precursor of human cytochrome *c* oxidase (Cox-VIII) at the N-terminus) at *Bam*HI and *Xho*I RE sites and pcDNA3-Nano-lantern-H2B (a DNA-binding protein histone 2B (H2B) at the C-terminus) at *Bam*HI and *Eco*RI RE sites (Saito et al., 2012). For peroxisome expression, we inserted the PCR-amplified Gamillus sequence with SKL (a peroxisome localization sequence) at the N-terminus into the pcDNA3 vector at *Bam*HI and *Eco*RI RE sites. For plasma membrane and Golgi complex expression we replaced the Phamlet sequence with the Gamillus sequence in pcDNA3-lyn-Phamlet (a myristoylation and palmitoylation sequence from lyn kinase at N terminus) at *Bam*HI and *Eco*RI RE sites and pcDNA3-Golgi-Phamret (β1,4-galactosyl- transferase) at *Bam*HI and *Eco*RI RE sites (Matsuda et al., 2008). For paxillin and zyxin localization, the Kohinoor sequence was replaced with the Gamillus sequence in pcDNA3-paxillin-Kohinoor and pcDNA3-zyxin-Kohinoor at *Bam*HI and *Kpn*I RE sites (Tiwari et al., 2015). For β-actin localization, the Kohinoor sequence was replaced with the Gamillus sequence in pcDNA3-Kohinoor-β-actin at *Hind*III and *Kpn*I RE sites. The open reading frames of paxillin and zyxin included a 17-amino-acids linker peptide (GTGSGGGGSGGGGSGGS), and β-actin included a 20 amino acids-long linker peptide (GGSGGSGGSGGSGGEFQ). For β-tubulin and nuclear localization, we replaced the Kohinoor sequence with the Gamillus sequence in pEGFP-N1-β-tubulin-Kohinoor at *Sal*I and *Not*I, and pcDNA3-Kohinoor-fibrillarin at *Bam*HI and *Eco*RI RE sites. A 21 amino acids-long linker (QSTGSGGGGSGGSTVPRARDP) was inserted between the Gamillus and β-tubulin sequences. For LAMP1 localization, we replaced the eNano-lantern sequence with the Gamillus sequence in pcDNA3-LAMP1-eNano-lantern at *Bam*HI and *Eco*RI RE sites (Suzuki et al., 2016). A 17 amino acids-long linker (GTGSGGGGSGGGGSGGS) was inserted between the LAMP1 and the Gamillus sequences. For LAMP3 localization, we inserted the PCR-amplified Gamillus sequence between the 44th and 45th amino acids of the LAMP3 sequence with *Bgl*II and *Age*I RE sites. The LAMP3 sequence was inserted into the pcDNA3 vector at *Bam*HI and *Eco*RI RE sites. For autophagosome expression, the PCR-amplified Gamillus sequence with *Bam*HI and *Bgl*II ends and the PCR-amplified LC3 sequence with *Bgl*II and *Eco*RI ends were ligated into pcDNA3 vector at *Bam*HI and *Eco*RI RE sites. For secretory vesicle expression, the PCR-amplified VAMP2 sequence with *Bam*HI and *Not*I ends and the PCR-amplified Gamillus sequence with *Not*I and *Eco*RI ends were ligated into pcDNA3 vector at *Bam*HI and *Eco*RI RE sites. For LifeAct localization, the PCR-amplified Gamillus and LifeAct sequences were inserted into pcDNA3 vector at *Bam*HI and *Eco*RI RE sites. The cDNAs of LAMP3, LC3, and VAMP2 were amplified from the plasmids, pCMV-lyso-pHluorin, pmRFP-LC3 (Kimura et al., 2007), and pEGFP-VAMP2 (Martinez-Arca et al., 2003) respectively (Addgene, plasmid #70113, #21075, and #42308 respectively).

Microscopy

For wide-field fluorescence imaging an inverted microscope (Eclipse Ti, Nikon) equipped with a 60× oil-immersion objective lens (NA = 1.40, Plan Apo, Nikon), 20× objective lens (NA = 0.45, Nikon) or 10× objective lens (NA = 0.30, Nikon) was used. A sCMOS camera (ORCA-flash4.0, C11440, Hamamatsu) or an electron-multiplying charge-coupled device (EMCCD) iXon Ultra camera (Andor) was used as the detector. For confocal fluorescence imaging, a microscope (FV1000, Olympus or A1, Nikon) equipped with a 60× oil-immersion lens (NA = 1.35, UPlanSApo, Olympus, or NA = 1.40, Plan Apo, Nikon) was used.

Photochromic Behavior

HeLa cells expressing Gamillus, and Gamillus-lysosomes (LAMP3) were prepared. The cells were illuminated using a mercury arc lamp (Intensilight C-HGFIE, Nikon) through a FF-01-370/36-25 bandpass filter (Semrock) for 10 s, and using a mercury arc lamp through a 465AF30 (XF3078), FF-02-472/30-25 or FF-01-500/25-24 bandpass filter (Semrock) for 40 s. Fluorescence images were detected through a FF01-520/35-25 or FF01-542/27-25 bandpass filter (Semrock) with 2 s intervals.

Photobleaching Measurement

HeLa cells expressing Gamillus or EGFP in the cytosol were prepared. The cells were maintained at 37°C during measurements. Photobleaching measurements were taken under continuous mercury lamp illumination through a 465AF30 bandpass filter (XF3078, Semrock) with 3.7 W/cm^2 power density. Images were taken for 10 min with 10 s intervals. Data collected from 16 cells were normalized by their initial values and averaged. The photobleaching halftime for FPs was calculated by fitting the data to a single exponential decay equation using Origin8 software.

OSER Assay

DNA constructs for the OSER assay were created by replacing mScarlet_N1 sequence between *Age*I and *Not*I RE sites in pCytERM_mScarlet_N1 (Addgene plasmid #85066) with EGFP, Gamillus or mNeonGreen sequence. HeLa cells transfected with each plasmid, by using lipofectamin 2000 were cultured for 16-18 hours before imaging. The fluorescence images were taken by a confocal microscope (FV1000, Olympus) with a 60× oil-immersion lens (NA = 1.35).

Cytotoxicity Measurement

HeLa cells at 20-30% confluency on a 24-well plate were transfected with pcDNA3-Gamillus or pcDNA3-EGFP by calcium phosphate method. One day after transfection, the medium was exchanged to fresh DMEM supplemented with 10% FBS and 1% penicillin/streptomycin, and the plate was set on a inverted microscope (Eclipse Ti, Nikon) equipped with a 10× objective lens (NA = 0.30), a motorized XY scanning stage (MLS203-1, Thorlabs) and a stage top incubator (Tokai Hit) maintaining culture atmosphere at 37°C and 5% CO_2. Time-lapse fluorescence images of multiple cells in different field of view were acquired every 12 hours for 2 days by using position registration function of MetaMorph Multi-Dimensional Acquisition module (Molecular Devices). Number of the fluorescent cell was counted manually.

Fluorescence Localization Imaging

HeLa cells expressing Gamillus fusions were imaged by a confocal microscope with an argon-ion laser light source (488 nm).

Comparison of Brightness of FP in Cells

HeLa cells expressing Gamillus or EGFP were prepared as is described in the "Cytotoxicity measurement" section. 1.5 days after transfection, fluorescence images were collected using a inverted microscope (Eclipse Ti, Nikon) with a 20× objective lens (NA = 0.45). For quantitative comparison of the brightness, average fluorescence intensity of hundreds of individual cells was extracted from acquired images by manually setting ROI using ImageJ software, and a histogram of the intensity was created.

Characterization of FPs in Lysosomes

HeLa cells expressing Gamillus or EGFP fused with LAMP3 were prepared. To check their lysosomal localization, the cells were incubated with 50 nM LysoTracker Red DND-99 (Thermo Fisher Scientific) for 1 h according to the manufacture's recommended protocol. The cells were illuminated by a mercy arc lamp with a FF01-562/40-25 bandpass filter (Semrock) and fluorescence was recorded with a FF02-641/75-25 bandpass filter (Semrock). Merged images were made using MetaMorph software (Molecular Devices). For quantitative comparison of the brightness between EGFP and Gamilus, average fluorescence intensity of hundreds of individual cells was extracted from acquired images by manually setting ROI using ImageJ software, and a histogram of the intensity was created. To check pH sensitivity, HeLa cells expressing Gamillus or EGFP fused with LAMP3 were treated with 30 mM ammonium chloride alkalization reagents (Christensen et al., 2002). The time-lapse images were recorded with 2 s intervals.

Imaging of Macroautophagy

For time-lapse imaging of macroautophagic events, HeLa cells were transfected with pcDNA3-Gamillus and cultured in DMEM with 10% FBS for ~36 h. The cells were maintained at 37°C with 5% CO_2 supply during imaging. Time-lapse imaging was performed using a wide-field microscope for ~30 h with 30 min intervals between image acquisition. The cells were excited by a mercury lamp with a 440–480 nm bandpass filter during acquisition, and fluorescence was detected using a 505-535 nm (FF01-520/35-25, Semrock) bandpass filter. Data were analyzed using ImageJ and MetaMorph software (Molecular Devices). To assess the lysosomal localization of FPs accumulated by macroautophagy the cells were incubated with 50 nM LysoTracker Red DND-99 for 1 h according to the manufacturer's recommended protocols. Scanning confocal fluorescence images were taken using an argon-ion laser (562 and 488 nm) or semiconductor laser (405 nm).

QUANTIFICATION AND STATISTICAL ANALYSIS

Data fitting or statistical analysis were performed using an Origin 8 software (OriginLab) or Microsoft Excel. Statistical values including the exact n and statistical significance are reported in Figure legends. Statistics of data collection for the X-ray crystallography experiment are listed in Table S2.

DATA AND SOFTWARE AVAILABILITY

The nucleotide sequence data of dfGFP and Gamillus was deposited on DNA Data Bank of Japan (DDBJ) with accession number of LC309248 and LC309249 respectively. The crystallographic data for Gamillus is deposited on Protein Data Bank Japan (PDBj) with the deposition numbers 5Y00 (https://pdbj.org/status-search?pdbid=5y00&sortBy=1) and 5Y01 (https://pdbj.org/status-search?pdbid=5y01).